Emission spectra of Cs-He excimers in cold helium gas

AUTHOR(S):

Enomoto, K; Hirano, K; Kumakura, M; Takahashi, Y; Yabuzaki, T

PHYSICAL REVIEW A **66**, 042505 (2002)

Emission spectra of Cs-He excimers in cold helium gas

K. Enomoto,* K. Hirano, M. Kumakura, Y. Takahashi, and T. Yabuzaki
Department of Physics, Graduate School of Science, Kyoto University, Kyoto 606-8502, Japan
(Received 27 April 2002; published 15 October 2002)

We observed broadband emission spectra of Cs-He excimers (Cs*He) in cold He gas (1.3–100 K), when Cs atoms were excited to the $6\,^2P$ states. We calculated the emission spectrum from each vibrational state of Cs*He using Pascale's semiempirical Cs-He potential energy curves [J. Pascale, Phys. Rev. A **28**, 632 (1983)], and compared the results with the observed spectra. From the measured spectral shape, we estimated the relative populations of the vibrational states of Cs*He at various He gas densities, and estimated the predissociation rate of Cs*He in the $A\,^2\Pi_{1/2}$ state. Moreover, a broadband emission spectrum of Cs*He_2 was also observed, which was compared with that observed in liquid He.

DOI: 10.1103/PhysRevA.66.042505 PACS number(s): 33.20.Ea, 34.30.+h, 67.40.Yv

I. INTRODUCTION

Alkali-metal atoms in gaseous He have been investigated by spectroscopic methods for a long time. The presence of He causes pressure broadening of resonance lines of alkali-metal atoms. The wide red wings of the *D* emission lines of alkali-metal atoms have been investigated extensively [1–6], and recently precise measurements of the pressure broadening of the Rb *D* absorption lines were reported by Romalis *et al.* [7]. These resonance line profiles were utilized to evaluate the alkali-metal–He interatomic potentials, which are difficult to determine precisely because of the weakness of the attractive interaction. However, clear observation of fluorescence from alkali-metal–He excimers and exciplexes, which leads to more precise evaluation of the interatomic potentials, has not occurred until recently. This is mainly because most of the experiments were carried out at or above room temperature, so that the thermal energy exceeded the small binding energy of alkali-metal and He atoms [for example, the potential well depth for the first excited state ($A^2\Pi$) is calculated to be 112 cm^{-1} for Cs-He [8]].

In the last decade, spectroscopic studies of alkali-metal atoms in cold He environments have made great progress [9], and exciplex formation in (or on) condensed He has been discussed to explain the unique features of the fluorescence. For example, in superfluid bulk liquid He, alkali-metal–He_n exciplex formation explained the absence of fluorescence from light alkali-metal atoms (Li,Na) [10–12], the absence of the D_2 line emission from excited Rb and Cs atoms [13], and the quenching of the Rb $5\,^2P_{1/2}$ state in pressurized liquid He [14]. Also, in solid He, Rb atoms do not emit visible fluorescence whereas Cs atoms do. Therefore, light absorption was used to detect nonfluorescing Rb atoms in a recent optical-rf double resonance experiment [15]. These interesting qualitative differences between different alkali-metal atoms can be explained in the context of the difference in spin-orbit coupling strength of the *P* state [12]. In liquid He, we observed infrared emission when heavy alkali-metal atoms (K,Rb,Cs) were excited to the first *P* state [16]. The emission is expected to be from the largest alkali-metal–$He_{n_{max}}$ exciplexes, where n_{max} represents the maximum number of He atoms bonding to an alkali-metal atom. The exciplex formation in liquid He is so rapid that transient exciplexes, such as Cs*He, have not been observed. Thus more dilute He environments are required for investigation of transient small exciplexes, to obtain information on the alkali-metal–He interatomic potentials and on the maximum number n_{max}. Recently, fluorescence from K*He_n, Na*He_n ($n=1,2$) [17], and Rb*He [18] was observed in such an environment. These exciplexes were produced by photodetachment from the surface of He nanodroplets. In these studies the observed spectra were compared with calculated spectra using Pascale's alkali-metal–He potentials [8]. Time resolved studies have also been reported [19,20], and Schulz *et al.* suggested that n_{max} for K-He exciplexes is 4, by observing the mass spectrum of exciplexes [20]. However, Cs*He has not been observed yet in spite of the interesting feature that it has a large difference from other alkali-metal atoms in the spin-orbit coupling strength. Thus we chose Cs, and we also intend to determine n_{max} for Cs-He exciplexes.

In the present work we have used the simplest environment of dilute He: cold He gas. This environment has an advantage over He nanodroplets, that is, we can change the temperature and the density of He gas over wide ranges. So far such a cold He gas has been used by Jakubek *et al.* for observing the fluorescence from Ag*He_n ($n=1,2$) [21].

In Sec. II we describe the experimental setup, and in Sec. III we show observed emission spectra of Cs*He_n ($n=1,2$). In Sec. IV we compare the measured spectra of Cs*He with theoretical ones calculated from the Cs-He potential curves reported by Pascale [8], and discuss the predissociation rate of Cs*He in the $A\,^2\Pi_{1/2}$ state. We also show an emission spectrum of Cs in liquid He.

II. EXPERIMENTAL SETUP

The experimental setup is illustrated in Fig. 1. The experiment was performed with a Pyrex glass cell (2 cm×2 cm ×3 cm rectangular solid) containing a small amount of Cs metal and He gas at a pressure of about 3.5 atm at room temperature (the density was about 9×10^{19} cm^{-3}). After the glass cell was evacuated to $\sim10^{-6}$ torr and baked at 500 K for about 20 h, Cs metal was transferred by distillation. To fill the cell with He gas at a high density, we immersed the

*Electronic address: enomoto@yagura.scphys.kyoto-u.ac.jp

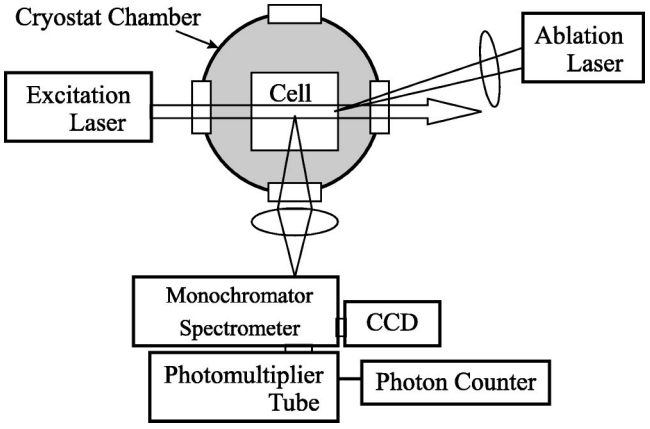

FIG. 1. Experimental setup.

cell in liquid nitrogen (77 K), introduced the He gas under 1 atm, and then sealed it off.

The cell was immersed in superfluid liquid He for cell temperatures $T<2.17$ K and it was placed in cold gaseous He for $T>2.17$ K, in a cryostat with optical windows. Below 1.9 K the He gas in the cell liquified. The He gas density was estimated from the saturated vapor pressure at a given temperature. Details of this cryostat chamber and the method of preparing cells have been described in Ref. [22].

To produce Cs vapor in the cold cell we adopted the laser ablation method; the second harmonic of pulsed Nd:$YLiF_4$ laser radiation (pulse energy 100 μJ, repetition rate 1 kHz, wavelength 523 nm) was focused on a small area of the cell wall, which was almost transparent but certainly covered with a thin film or small particles of Cs. After a few second irradiation, we obtained cold atomic Cs gas with a density of 10^8–10^{10} cm^{-3}. The increase of the cell temperature caused by the laser irradiation was measured to be less than 0.01 K for $T<1.9$ K and less than 0.5 K for $T>1.9$ K. This temperature increase was confirmed by observing the small broadening of the D_2 ($6\,^2S_{1/2}\rightarrow 6\,^2P_{3/2}$) excitation line. With respect to the preparation of cold alkali-metal atomic gas we previously reported the light-induced atom desorption (LIAD) method, which is a very effective way to produce cold gaseous atoms for Rb and K [22]. However, we did not adopt the LIAD method in the present work, because it is not efficient above the superfluid temperature and does not work effectively for Cs.

The gaseous Cs atoms produced were excited by a cw diode laser beam (typical intensity 1 mW/mm^2), which was tuned to the D_1 line ($6\,^2S_{1/2}\rightarrow 6\,^2P_{1/2}$) at 11 181 cm^{-1} (894.3 nm) or the D_2 line ($6\,^2S_{1/2}\rightarrow 6\,^2P_{3/2}$) at 11 736 cm^{-1} (852.1 nm). The fluorescence from a small volume in the excitation beam was introduced into a spectrometer and detected with a liquid-N_2-cooled charge coupled device (CCD) (Princeton Instruments, LN/CCD-1100PF). The resolution of the spectrometer-CCD system was about 16 cm^{-1} and the available spectral range was from the visible range to about 10 000 cm^{-1}. For the longer wavelength region (wave number down to 6250 cm^{-1}), we used an ir-sensitive photomultiplier tube (Hamamatsu, R5509-71) connected to a monochromator, with a resolution of about 60 cm^{-1}. The sensitivities of both detection systems were calibrated by using a commercial standard lamp.

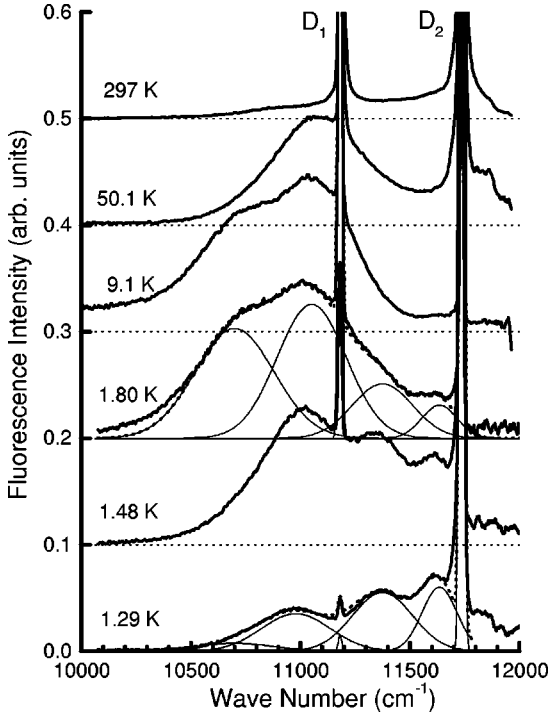

FIG. 2. Emission spectra in the case of D_2 excitation at various temperatures (thick lines). The superpositions (dotted lines) of six Gaussian curves (thin lines) are fitted to the observed spectra at 1.29 K and 1.80 K. Above 1.9 K the He gas density was 9×10^{19} cm^{-3}, and below 1.9 K it was given by the saturated vapor pressure: 6.7×10^{19} cm^{-3} at 1.80 K, 2.1×10^{19} cm^{-3} at 1.48 K, and 8.4×10^{18} cm^{-3} at 1.29 K.

To observe the emission spectrum in liquid He, we immersed bulk Cs metal in liquid He at 1.6 K, and sputtered its surface with the pulsed Nd:$YLiF_4$ laser (100 μJ/pulse, 523 nm). Following a dark period of 50 μs after each sputtering pulse, a chopped cw Ti:Al_2O_3 laser excited the produced Cs atoms through the D_2 line [intensity $\sim$300 mW/mm^2, wave number 12 034 cm^{-1} (831.0 nm)].

III. OBSERVED EMISSION SPECTRA

The laser-induced fluorescence spectra observed through D_2 excitation (11 736 cm^{-1}) at various temperatures are shown in Fig. 2. The spectra shown have been normalized by the total fluorescence intensity integrated over the observed wave number range. As reported in Ref. [1], at room temperature we observed only the D lines of atomic Cs with wide wings. However, at low temperatures ($T<100$ K), a broad spectrum ranging from the D_2 line to about 10 300 cm^{-1} was clearly observed. This is the spectrum of Cs*He excimers as discussed in Sec. IV C. A weak red wing around 10 000 cm^{-1} observed at 3–15 K is from Cs*He_2 as discussed later.

The observed spectral profile was found to depend strongly on the temperature T below 1.9 K, where the gaseous He density in the cell changed drastically with T. The

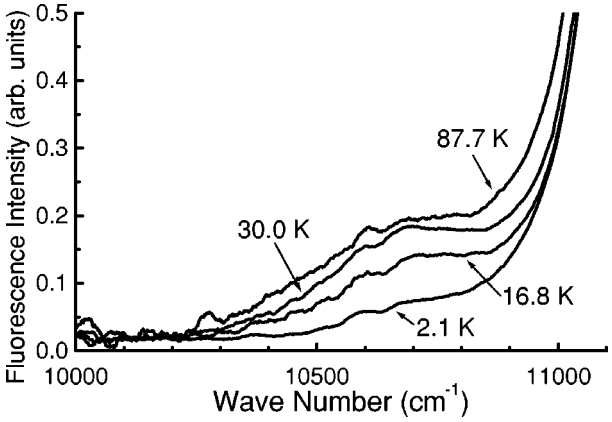

FIG. 3. Emission spectra in the case of D_1 excitation at various temperatures. They are normalized by the peak intensity of the D_1 emission line.

observed spectra were composed of four broad components and two atomic D_1 and D_2 lines, so that we fitted the superposition of six Gaussian curves to the observed spectra, as shown in Fig. 2. We found that the center wave numbers of the four broad Gaussian curves were about 10 695 cm^{-1}, 11 070 cm^{-1}, 11 380 cm^{-1}, and 11 635 cm^{-1}, and the full widths at half maximum (FWHMs) were, respectively, about 440 cm^{-1}, 390 cm^{-1}, 295 cm^{-1}, and 190 cm^{-1}. Comparing these four best-fitted Gaussians at the temperatures 1.80 K and 1.29 K, we found that the positions and widths of the four components did not change, in spite of large changes of the spectral profile, except for a slight red shift (-80 cm^{-1}) of the component at 11 070 cm^{-1} with decreasing T. These broad components correspond to the emission spectra from the vibrational states of Cs*He, as discussed in Sec. IV C. At about 1.9 K the components at 10 695 cm^{-1} and 11 070 cm^{-1} were dominant, and at about 1.3 K the former component became very weak. As the temperature increased from 1.9 K, the former component decreased fast and the latter decreased slowly. The ratio of the total intensity of the emission from Cs*He to that of the D lines from Cs gradually decreased, for example, it was 3.8 at 2.1 K and 0.7 at 50 K, although the He gas density was constant (9×10^{19} cm^{-3}).

We observed also the fluorescence induced by D_1 excitation (11 181 cm^{-1}). In this case a very weak broad component was observed on the red wing of the D_1 line at temperatures above 10 K (Fig. 3). No other emission line was observed. At temperatures below 10 K the emission spectra were almost the same as that at 2.1 K. With increasing T, the intensity of the broad component became larger, and the fraction of the broadband emission in the total emission intensity had the maximum value ~0.01 at 35 K. For $T>35$ K it gradually merged into the wing of the D_1 line. This component had almost the same position and width as those of the spectral component at 10 695 cm^{-1} observed in the D_2 excitation case. This is the emission from Cs*He in the $A\,^2\Pi_{1/2}$ state, as discussed in Sec. IV B.

We also paid attention to the red wing of the Cs*He spectra in the range of 9500–10500 cm^{-1} observed in the case of D_2 excitation. Figure 4 shows the red wing at 2.1 K and 6.6

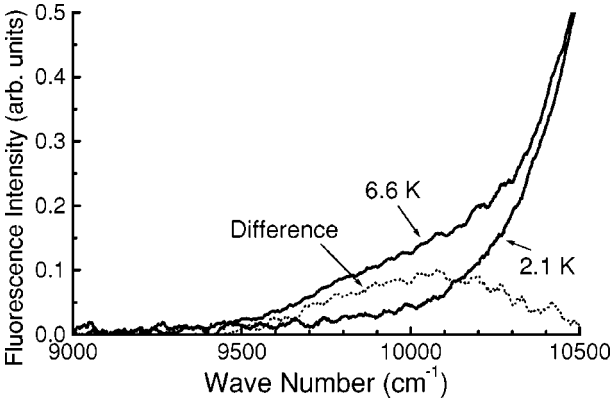

FIG. 4. Emission spectra in an infrared region at 6.6 K and 2.1 K (solid lines) in the case of D_2 excitation. They are normalized by the intensity of the spectral component at 10 695 cm^{-1}. The dotted line shows the difference between these two spectra.

K, where we see the existence of a weak spectral component around 10 000 cm^{-1} at 6.6 K. This line was observed only in the temperature range from 3 K to 15 K. By subtracting the spectrum at 2.1 K from that at 6.6 K, we found the peak of the line was at 10 045 cm^{-1} and the width was 610 cm^{-1}. The integrated intensity of this line relative to the total fluorescence intensity was ~0.05.

A similar broadband emission spectrum, with a peak at 10 050 cm^{-1} and a width of 620 cm^{-1}, was observed in liquid He as shown in Fig. 5, where we also see the narrow D_1 line. No other spectral component was observed in the wave number range down to 6250 cm^{-1}. The integrated intensity of the broad line was ~0.97 relative to the total fluorescence intensity. This line around 10 000 cm^{-1} is assigned to be the emission from Cs^*He_2 as discussed in Sec. IV E.

IV. ANALYSIS AND DISCUSSION

A. Calculation of the emission spectra of Cs*He

We considered that the observed emission spectra in cold He gas were from Cs^*He_n ($n=1,2$) exciplexes, and that the

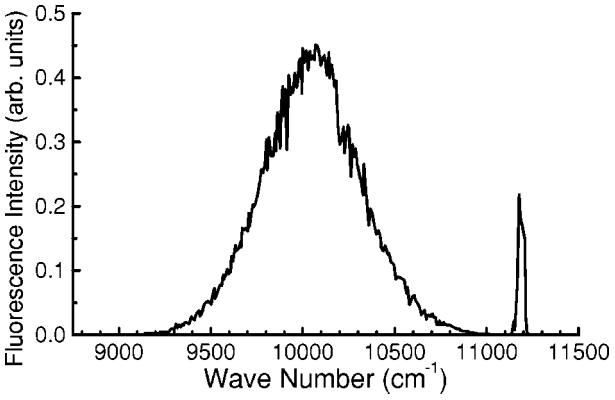

FIG. 5. Emission spectrum of Cs atoms excited through the D_2 transition (12 034 cm^{-1}) in superfluid liquid He at 1.6 K. The broad component at about 10 050 cm^{-1} is assigned to be the emission from Cs^*He_2 and the narrow one at 11 210 cm^{-1} is the D_1 emission line of Cs.

undulating structure in the case of D_2 excitation was superposition of the emission spectra from different vibrational states of Cs*He. To confirm them, we calculated the emission spectra of Cs*He under the Franck-Condon approximation, using Pascale's semiempirical interatomic potentials [8]. Since these potentials are spin-orbit averaged ones, we must take account of the spin-orbit interaction, which is stronger than the interaction between He and Cs($6\,^2P$) at the equilibrium internuclear distance. The method we used is the same as that in Refs. [23,24]. The potential curves relevant to the Cs($6\,^2P$)+He($1\,^1S_0$) atomic system are for the $A\,^2\Pi$ and $B\,^2\Sigma$ states which are well expressed in the $|LSL_zS_z\rangle$ representation. The spin-orbit interaction is, however, diagonal in the $|LSJJ_z\rangle$ representation. The total interaction Hamiltonian can be written in terms of the bases $[B\,^2\Sigma_{1/2}, A\,^2\Pi_{1/2}, A\,^2\Pi_{3/2}]$ as

$$\begin{bmatrix} V_\Sigma(R) & \frac{\sqrt{2}}{3}\Delta_{SO} & 0 \\ \frac{\sqrt{2}}{3}\Delta_{SO} & V_\Pi(R)-\frac{\Delta_{SO}}{3} & 0 \\ 0 & 0 & V_\Pi(R)+\frac{\Delta_{SO}}{3} \end{bmatrix}, \qquad (1)$$

where Δ_{SO} is the spin-orbit splitting energy of Cs in the $6\,^2P$ states (554.04 cm^{-1}), R is the Cs-He internuclear distance, and $V_\Pi(R)$ and $V_\Sigma(R)$ are the potential energies for the $A\,^2\Pi$ and $B\,^2\Sigma$ states, respectively. This method is based on the assumption that the spin-orbit coupling strength is independent of R.

Diagonalizing the matrix (1) for each R, we obtained the potential curves of Cs-He as shown in Fig. 6, where the ground state potential curve is also shown. They are labeled by the dominant $|LSL_zS_z\rangle$ component at small R. The potential curve with the highest energy among the three excited states is that for the $B\,^2\Sigma_{1/2}$ state which correlates with Cs($6\,^2P_{3/2}$)+He($1\,^1S_0$). This potential curve does not have a well deep enough to make a bound or quasibound state. The middle potential curve is for the $A\,^2\Pi_{3/2}$ state correlating with Cs($6\,^2P_{3/2}$)+He($1\,^1S_0$). This potential curve has a well at $R=3.5$ Å with a depth of 112 cm^{-1} measured from the dissociation limit and has no potential barrier. The lowest potential curve is for the $A\,^2\Pi_{1/2}$ state correlating with Cs($6\,^2P_{1/2}$)+He($1\,^1S_0$). This potential has a barrier at $R=5.0$ Å with a height of 75.2 cm^{-1} measured from the dissociation limit and has a well at $R=3.5$ Å with a depth of 52.2 cm^{-1} from the peak of the barrier. The potential curve for the ground state $X\,^2\Sigma_{1/2}$ is almost repulsive [8].

We calculated the vibrational eigenfunctions $\psi'(R)$ and eigenenergies for the $A\,^2\Pi_{1/2}$ and $A\,^2\Pi_{3/2}$ states. The calculations were performed with Le Roy's program code LEVEL 7.4 [25], which can numerically solve the one-dimensional Schrödinger equation with the Numerov-Cooley algorithm. The $A\,^2\Pi_{1/2}$ state has only one quasibound vibrational state (predissociating state) and the $A\,^2\Pi_{3/2}$ state has five bound vibrational states. The energies of these vibrational states are listed in Table I and are also shown as dotted lines in Fig. 6.

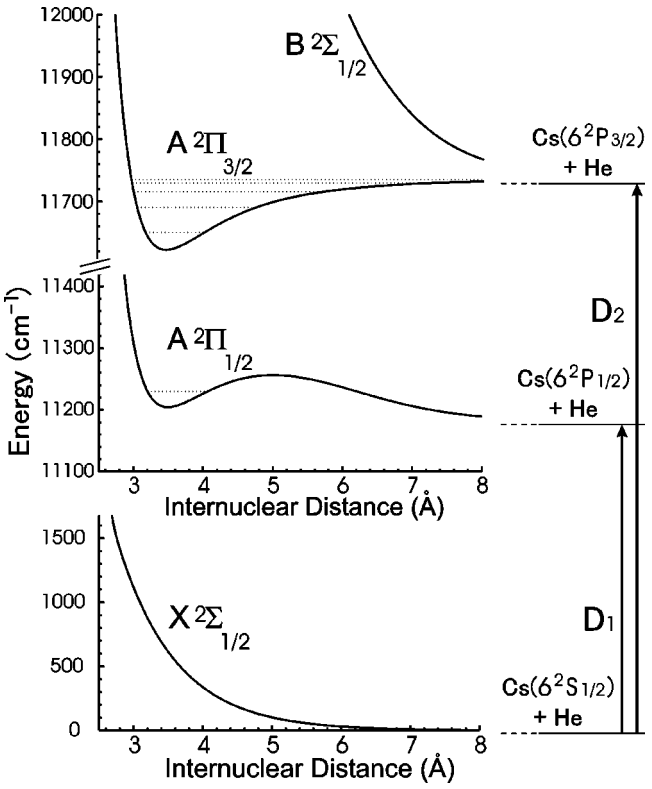

FIG. 6. Cs-He potential curves including the spin-orbit interaction (solid lines). The dotted lines show the vibrational energy levels. The electronic state of the separated atomic pair is also shown for each molecular electronic state.

The emission spectra $I(\nu)$ for the transitions from the vibrational states of these two $A\,^2\Pi$ states to the ground state $X\,^2\Sigma_{1/2}$ were calculated under the Franck-Condon approximation: $I(\nu)\propto\nu^3\left|\int dR\,\psi(R;\nu)\psi'(R)\right|^2$, where ν is the transition frequency, and $\psi(R;\nu)$ is the wave function of the electronic ground state. We have neglected their rotational structure. The calculated spectra are shown in Fig. 7. We compare these theoretical spectra with the observed ones in Secs. IV B and IV C.

B. Emission spectra in the case of D_1 excitation

In the case of D_1 excitation, we observed only the D_1 emission line of Cs and a very weak broad spectral compo-

TABLE I. Energies of the vibrational states of Cs*He (v is the vibrational quantum number). These values are relative to the energies of Cs($6\,^2P_{1/2}$)+He($1\,^1S_0$) and Cs($6\,^2P_{3/2}$)+He($1\,^1S_0$) for the $A\,^2\Pi_{1/2}$ and $A\,^2\Pi_{3/2}$ states, respectively. The state with a positive energy is a quasibound state.

Vibrational state	Energy (cm^{-1})
$A\,^2\Pi_{1/2}$ $v=0$	48.35
$A\,^2\Pi_{3/2}$ $v=0$	−84.89
$v=1$	−45.09
$v=2$	−19.79
$v=3$	−5.90
$v=4$	−0.51

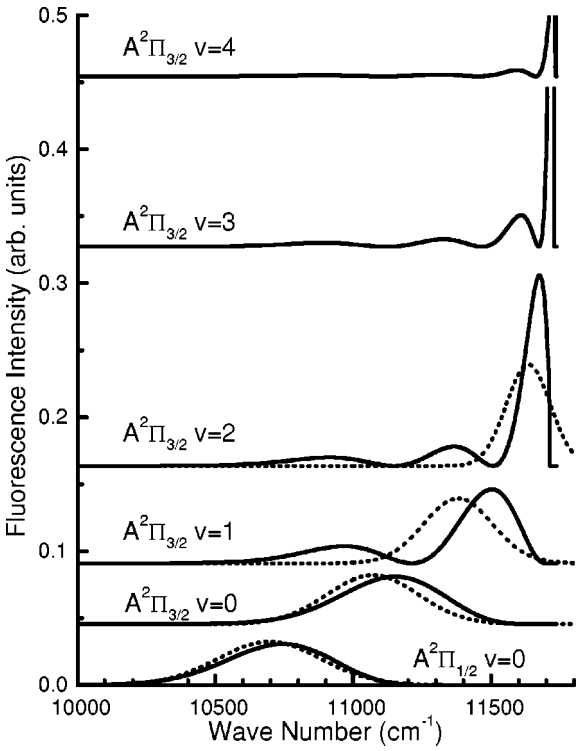

FIG. 7. Calculated emission spectra of Cs*He in the $A\,^2\Pi_{1/2}\,v=0$ and $A\,^2\Pi_{3/2}\,v=0-4$ states (solid lines). The relative population of each state is normalized. The dotted lines show the Gaussian curves used in Fig. 2 (see Sec. IV C).

nent around 10 695 cm^{-1}, as seen in Fig. 3. These two components overlapped each other, so that in order to obtain the broad spectral component distinctively, we subtracted the D_1 emission line (the spectrum at 2.1 K) from the spectrum observed at 30.0 K. The resultant broad component is shown in Fig. 8. This broad component is quite similar to the theoretical spectrum for the $A\,^2\Pi_{1/2}\,v=0\rightarrow X\,^2\Sigma_{1/2}$ transition, which is shown by the dotted line in Fig. 8. Thus we can conclude that this broadband emission is from Cs*He in the $A\,^2\Pi_{1/2}\,v=0$ state. The peak position of the theoretical spectrum deviates from that of the observed one by about 50 cm^{-1} toward larger wave number. This deviation can be attributed to errors in the potential calculation. The integrated intensity of this broadband emission was much smaller than that observed in the case of D_2 excitation. This is ascribed mainly to the existence of the potential barrier for the $A\,^2\Pi_{1/2}$ state.

Note that the $A\,^2\Pi_{1/2}$ state has only one vibrational state according to our calculation. Therefore we can clearly conclude that the observed broad spectral component can be assigned uniquely to the $A\,^2\Pi_{1/2}\,v=0\rightarrow X\,^2\Sigma_{1/2}$ transition. This favorable situation is not realized for Na*He [17], K*He [17], Rb*He [18], or even Cs*He in the $A\,^2\Pi_{3/2}$ state. Emission spectra of these excimers are superpositions of the components from several vibrational states, which overlap one another. Thus it is difficult to decompose it into individual components.

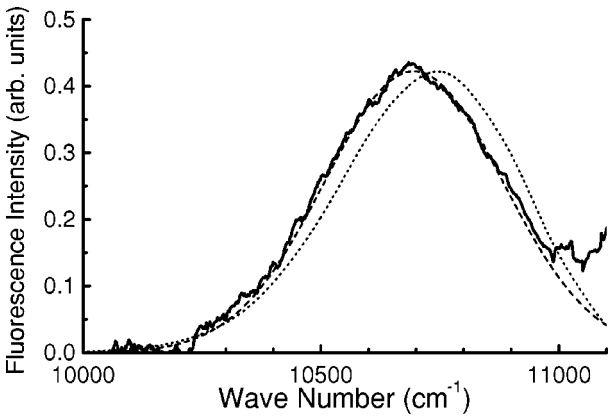

FIG. 8. Emission spectrum of Cs*He in the $A\,^2\Pi_{1/2}$ state. The solid line shows the difference between the spectra observed at 30.0 K and 2.1 K in the case of D_1 excitation (see Fig. 3). The dotted line shows the theoretical spectrum. The dashed line shows the Gaussian curve with a peak at 10 695 cm^{-1} used in Fig. 2.

C. Emission spectra of Cs*He in the case of D_2 excitation

When Cs atoms were excited through the D_2 line, we observed that the emission spectrum consisted of several broad spectral components. This emission spectrum is well expressed by the superposition of the six Gaussian functions shown in Fig. 2. Comparing these Gaussian curves with the theoretical spectra calculated in Sec. IV A, we found that the four broad components centered at 10 695 cm^{-1}, 11 070 cm^{-1}, 11 380 cm^{-1}, and 11 635 cm^{-1} correspond to the emission from the $A\,^2\Pi_{1/2}\,v=0$, $A\,^2\Pi_{3/2}\,v=0$, $A\,^2\Pi_{3/2}\,v=1$, and $A\,^2\Pi_{3/2}\,v=2$ states of Cs*He, respectively (see Fig. 7). It must be noted that there exist deviations of the peak positions between the experimental spectra and the corresponding theoretical ones. In any case, the theoretical peak is located on the high energy side of the experimental one. We believe, however, that there is no ambiguity in the above assignment, because all deviations are relatively small (<125 cm^{-1}). Furthermore, the component at 10 695 cm^{-1} has already been assigned independently from the experimental result in the case of D_1 excitation, as mentioned in Sec. IV B. The deviations probably result from the lack of precision in the pair potential curves of Cs-He. The emission spectra from the $A\,^2\Pi_{3/2}\,v\geqslant 3$ states are almost merged with the red wing of the D_2 line, and thus we cannot distinguish these components.

As described in Sec. III, we observed a slight redshift of the component at about 11 070 cm^{-1} with decreasing T. We consider that this peak shift is caused by the fact that the spectrum from the $A\,^2\Pi_{3/2}\,v=0$ state almost overlaps a minor component of the spectrum from the $v=1$ state located at slightly smaller wave number (see the calculated spectra from the $v=0$ and $v=1$ states shown in Fig. 7). As mentioned in Sec. IV D, with decreasing T, the population of the $v=1$ state increases relative to that of the $v=0$ state, and it results in the redshift.

D. Population distribution among vibrational states

Here, we estimate the relative populations of vibrational states of the $A\,^2\Pi_{1/2}$ and $A\,^2\Pi_{3/2}$ states at various tempera-

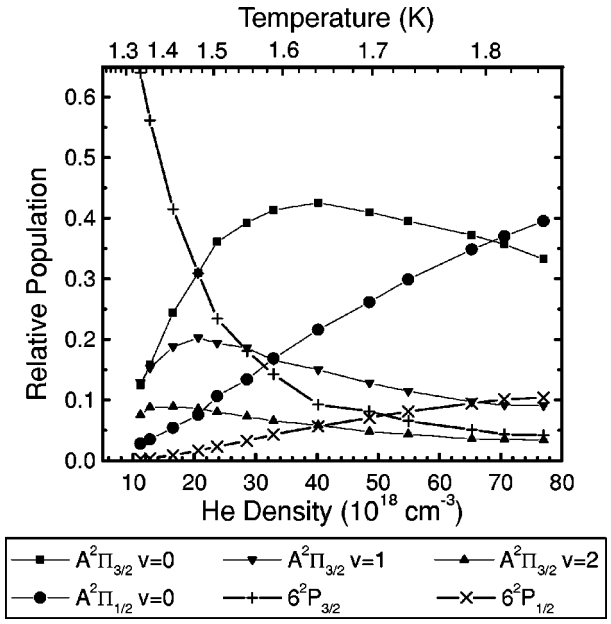

FIG. 9. He gas density dependence of the relative populations of the vibrational states of Cs*He and the $6\,^2P$ states of Cs (dots with solid lines). The cell temperature corresponding to the He gas density is shown as the upper abscissa.

tures between 1.34 K and 1.83 K, in the case of D_2 excitation. We assumed that each best-fitted Gaussian curve $g_i(\nu)$ $(i=1-6)$ corresponds to the strongest component of the emission spectrum from a vibrational state of Cs*He and to the Cs D_1 and D_2 lines. We estimated the relative population of each state as $\int g_i(\nu)\nu^{-3}d\nu$, assuming that the electronic transition moment of Cs*He($A\,^2\Pi\rightarrow X\,^2\Sigma$) is equal to that of Cs($6\,^2P\rightarrow 6\,^2S$).

Figure 9 shows the obtained relative populations of the vibrational states of Cs*He and the $6\,^2P_{1/2}$ and $6\,^2P_{3/2}$ states of Cs at temperatures between 1.34 K and 1.83 K. In this temperature range the He gas density changes by a factor of about 7. At about 1.34 K, where the number density of He atoms is about 1×10^{19} cm^{-3}, D_2 excitation populates mainly the $A\,^2\Pi_{3/2}$ state of Cs*He ($\sim$46%) and the $6\,^2P_{3/2}$ state of Cs ($\sim$52%), and even high vibrational levels of the $A\,^2\Pi_{3/2}$ state are substantially populated. As the temperature goes up, the He gas density increases and the fraction of the population of Cs*He increases. Among several vibrational states of Cs*He, the populations of the $A\,^2\Pi_{1/2}$ $v=0$ and $A\,^2\Pi_{3/2}$ $v=0$ states become dominant, because the vibrational relaxation and the electronic $A\,^2\Pi_{3/2}\rightarrow A\,^2\Pi_{1/2}$ relaxation become faster, mainly due to the increase in the number of collisions. The strong density dependence of the population distribution indicates that these relaxation times are of the same order of the radiative lifetime of Cs*He in this density range (1×10^{19}–8×10^{19} cm^{-3}).

This density dependence gives us further interesting information concerning the predissociation from the $A\,^2\Pi_{1/2}$ $v=0$ state. The Cs($6\,^2P_{1/2}$) atom is created by three processes; the predissociation of Cs*He($A\,^2\Pi_{1/2}$) and the two collisional relaxations Cs($6\,^2P_{3/2}$)$\rightarrow$Cs($6\,^2P_{1/2}$) and Cs*He($A\,^2\Pi_{3/2}$)$\rightarrow$Cs($6\,^2P_{1/2}$)+He($1\,^1S_0$). On the other hand, the Cs($6\,^2P_{1/2}$) atom decays almost solely through the radiative transition. The other decay processes such as Cs($6\,^2P_{1/2}$)+He($1\,^1S_0$)$\rightarrow$Cs*He($A\,^2\Pi_{1/2}$) can be neglected because the emission from Cs*He after D_1 excitation was not observed below 10 K. In the steady state where the creation and decay rates are balanced, the predissociation rate $\gamma N_{\Pi 1/2}$, which is one of the creation rates, should be smaller than the spontaneous emission rate $\Gamma N_{P1/2}$ (that is, $\gamma<\Gamma N_{P1/2}/N_{\Pi 1/2}$), where $N_{P1/2}$ and $N_{\Pi 1/2}$ are the populations of Cs($6\,^2P_{1/2}$) and Cs*He($A\,^2\Pi_{1/2}$), respectively, γ is the rate constant for the predissociation of Cs*He($A\,^2\Pi_{1/2}$), and Γ is the radiative transition rate coefficient of Cs($6\,^2P_{1/2}$) (3.3×10^7 s^{-1}). The ratio $N_{P1/2}/N_{\Pi 1/2}$ is less than 0.27 and is almost constant above 1.6 K. This leads to the relation $\gamma<9.0\times10^6$ s^{-1}. This predissociation rate constant is much smaller than the value of 3.7×10^8 s^{-1}, calculated theoretically with the program LEVEL 7.4 [25]. This discrepancy implies that the real potential curve for the $A\,^2\Pi_{1/2}$ state has a larger potential barrier and/or a lower $v=0$ level than the calculated results.

E. Emission spectra of Cs*He$_2$ in gaseous and liquid He

The broad emission line at 10 045 cm^{-1} shown in Fig. 4 cannot be explained as fluorescence from Cs*He. As in cold He gas, we observed a similar broad line in liquid He through D_2 excitation (Fig. 5). In liquid He, the spectral components of the fluorescence from Cs*He were not observed, so that we conclude that this broad line is due to emission from Cs*He$_2$. This agrees well with the fact that the energy differences of this line from the atomic D_1 and D_2 lines are approximately twice the differences from the $A\,^2\Pi_{1/2}$ and $A\,^2\Pi_{3/2}$ Cs*He $v=0$ states, respectively. The formation of Cs*He$_2$ in liquid He was predicted by Dupont-Roc [12]. He pointed out that the valence electron of Cs($6\,^2P_{3/2}$) has an applelike wave function and that two He atoms at maximum can attach to the Cs($6\,^2P_{3/2}$) atom. This explanation agrees with our experimental result in liquid He. In He gas, the intensity of this broad line became maximum at temperatures 3–15 K, but the reason for this has not been found yet.

V. CONCLUSION

We have observed broadband emission spectra of Cs*He$_n$ $(n=1,2)$ exciplexes, by producing and exciting Cs atoms in cold He gas. We have assigned the spectra near the D lines to be from Cs*He, by calculating spectra under the Franck-Condon approximation using potential curves including the spin-orbit interaction. D_2 excitation leads to strong broadband emission from the $A\,^2\Pi_{3/2}$ and $A\,^2\Pi_{1/2}$ states of Cs*He, while D_1 excitation leads to very weak emission from the $A\,^2\Pi_{1/2}$ state. This difference between D_2 and D_1 excitation in the intensity of the broadband emission is due to the fact that the potential curve for the $A\,^2\Pi_{1/2}$ state has a potential barrier and no bound states except for a quasibound state. We have also estimated the relative populations of the vibrational states of Cs*He at various temperatures below 1.9 K, and have found that the vibrational and $A\,^2\Pi_{3/2}$

$\rightarrow A\,^2\Pi_{1/2}$ relaxation rates are comparable to the radiative transition rate. We have estimated the upper limit of the predissociation rate constant for Cs*He in the $A\,^2\Pi_{1/2}$ state to be 9.0×10^6 s^{-1}, which is two orders of magnitude smaller than the value calculated theoretically. This result as well as the deviations of the theoretical spectra from the experimental ones demand further improvement of the theoretical potential curves, especially for the excited states. The weak broad spectral component at about 10 045 cm^{-1} is from Cs^*He_2 exciplexes. It agrees very well with the spectrum observed in liquid He. Recently, a similar investigation for Rb in cold He gas was carried out and the result will be reported elsewhere.

ACKNOWLEDGMENTS

We acknowledge J. Pascale for giving us the numerical Cs-He pair potential curves, and R. J. Le Roy for use of his program for calculating vibrational levels of diatomic molecules and predissociation rates. We thank also A. Hatakeyama and T. Matsuura for their contribution in the early stage of the present work. This work was supported by a Grant-in-Aid for Scientific Research of Ministry of Education, Culture, Sports, Science, and Technology of Japan (Grant No. 11304023). One of the authors (K.E.) acknowledges support from the Japan Society for the Promotion of Science.

[1] R.E.M. Hedges, D.L. Drummond, and A. Gallagher, Phys. Rev. A **6**, 1519 (1972).
[2] D.L. Drummond and A. Gallagher, J. Chem. Phys. **60**, 3426 (1974).
[3] G. York, R. Scheps, and A. Gallagher, J. Chem. Phys. **63**, 1052 (1975).
[4] R. Scheps, Ch. Ottinger, G. York, and A. Gallagher, J. Chem. Phys. **63**, 2581 (1975).
[5] M.D. Havey, S.E. Frolking, and J.J. Wright, Phys. Rev. Lett. **45**, 1783 (1980).
[6] L.C. Balling, J.J. Wright, and M.D. Havey, Phys. Rev. A **26**, 1426 (1982).
[7] M.V. Romalis, E. Miron, and G.D. Cates, Phys. Rev. A **56**, 4569 (1997).
[8] J. Pascale, Phys. Rev. A **28**, 632 (1983).
[9] As reviews, see B. Tabbert, H. Günther, and G. zu Putlitz, J. Low Temp. Phys. **109**, 653 (1997); S.I. Kanorsky and A. Weis, Adv. At., Mol., Opt. Phys. **38**, 87 (1997).
[10] Y. Takahashi, K. Sano, T. Kinoshita, and T. Yabuzaki, Phys. Rev. Lett. **71**, 1035 (1993).
[11] S. Kanorsky, A. Weis, M. Arndt, R. Dziewior, and T.W. Hänsch, Z. Phys. B: Condens. Matter **98**, 371 (1995).
[12] J. Dupont-Roc, Z. Phys. B: Condens. Matter **98**, 383 (1995).
[13] T. Kinoshita, K. Fukuda, Y. Takahashi, and T. Yabuzaki, Phys. Rev. A **52**, 2707 (1995).
[14] T. Kinoshita, K. Fukuda, T. Matsuura, and T. Yabuzaki, Phys. Rev. A **53**, 4054 (1996).
[15] T. Eichler, R. Müller-Siebert, D. Nettels, S. Kanorsky, and A. Weis, Phys. Rev. Lett. **88**, 123002 (2002).
[16] As preliminary data we observed such infrared fluorescence. For Rb and K, broad emission spectra around 7000 cm^{-1} were observed.
[17] J. Reho, J. Higgins, C. Callegari, K.K. Lehmann, and G. Scoles, J. Chem. Phys. **113**, 9686 (2000).
[18] F.R. Brühl, R.A. Trasca, and W.E. Ernst, J. Chem. Phys. **115**, 10220 (2001).
[19] J. Reho, J. Higgins, K.K. Lehmann, and G. Scoles, J. Chem. Phys. **113**, 9694 (2000).
[20] C.P. Schulz, P. Claas, and F. Stienkemeier, Phys. Rev. Lett. **87**, 153401 (2001).
[21] Z.J. Jakubek, Q. Hui, and M. Takami, Phys. Rev. Lett. **79**, 629 (1997).
[22] A. Hatakeyama, K. Enomoto, N. Sugimoto, and T. Yabuzaki, Phys. Rev. A **65**, 022904 (2002).
[23] J.S. Cohen and B. Schneider, J. Chem. Phys. **61**, 3230 (1974).
[24] Z.J. Jakubek and M. Takami, Chem. Phys. Lett. **265**, 653 (1997).
[25] R. J. Le Roy, University of Waterloo Chemical Physics Research Report No. CP-642R 2001 (unpublished).